

Parallel performance of shared memory parallel spectral deferred corrections^{*}

Philip Freese¹[0000-0002-9838-6321], Sebastian Götschel¹[0000-0003-0287-2120],
Thibaut Lunet¹[0000-0003-1745-0780], Daniel Ruprecht¹[0000-0003-1904-2473],
and Martin Schreiber²[0000-0002-2390-6716]

- ¹ Institute of Mathematics, Hamburg University of Technology, Hamburg, Germany
{philip.freese,sebastian.goetschel,thibaut.lunet,ruprecht}@tuhh.de
² Univ. Grenoble Alpes / Laboratoire Jean Kuntzmann / Inria, Grenoble, France
Technical University of Munich, Germany
martin.schreiber@univ-grenoble-alpes.fr

Abstract. We investigate parallel performance of parallel spectral deferred corrections, a numerical approach that provides small-scale parallelism for the numerical solution of initial value problems. The scheme is applied to the shallow water equation and uses an IMEX splitting that integrates fast modes implicitly and slow modes explicitly in order to be efficient. We describe parallel `OpenMP`-based implementations of parallel SDC in two well established simulation codes: the finite volume based operational ocean model `ICON-0` and the spherical harmonics based research code `SWEET`. The implementations are benchmarked on a single node of the `JUSUF (SWEET)` and `JUWELS (ICON-0)` system at Jülich Supercomputing Centre. We demonstrate a reduction of time-to-solution across a range of accuracies. For `ICON-0`, we show speedup over the currently used Adams–Bashforth-2 integrator with `OpenMP` loop parallelization. For `SWEET`, we show speedup over serial spectral deferred corrections and a second order implicit-explicit integrator.

Keywords: parallel-in-time methods · spectral deferred corrections · shared-memory parallelization · shallow water equations · hyperbolic equation

1 Introduction

Parallel-in-time integration methods can provide additional concurrency when solving initial value problems on massively parallel computers. Given the ongoing rapid increase in the number of cores in state-of-the-art high-performance

^{*} This project received funding from the German Federal Ministry of Education and Research (BMBF) under grant 16ME0679K. Supported by the European Union - NextGenerationEU. This project has also received funding from the European High-Performance Computing Joint Undertaking (JU) under grant agreement No 955701. The JU receives support from the European Union’s Horizon 2020 research and innovation programme and Belgium, France, Germany, and Switzerland. This project also received funding from the German Federal Ministry of Education and Research (BMBF) grant 16HPC048.

computing systems, spatial parallelization alone is unlikely going to be sufficient to translate computing power into application performance. In the terminology introduced by Gear [10], there are parallel-across-the-steps methods like Parareal [21], MGRIT [7] or PFASST [6] and parallel-across-the-method algorithms like Runge-Kutta methods with diagonal Butcher table [15], iterated Runge-Kutta methods [13] or parallel spectral deferred corrections (SDC) [28]. While the former can scale to a larger number of cores, they are more complicated to implement and require the use of a coarse model to handle information transport in time, which is costly in terms of developer time and also limits achievable speedup as it constitutes a serial bottleneck. By contrast, parallel-across-the-method algorithms are easier to implement and can theoretically provide ideal speedup. However, they are limited in the number of parallel processes they can use. Since SDC-based algorithms have already been successfully used in the context of earth system modeling [12,16,26], exploring the feasibility of using parallel SDC to speed up an operational model is a logical next step.

The contributions of this paper are: (i) a description of the successful integration of parallel SDC into a research code and an operational ocean model including a description of the necessary mathematical tweaks in the method, (ii) the first demonstration that parallel SDC can provide speedup on a single node of a state-of-the-art high-performance computing system and (iii) an illustration that a nested `OpenMP` variant with parallel SDC in the outer and fine-grained parallelism in the inner loop provides better performance than loop-parallelization of the mesh operations alone.

2 Related work

First attempts to construct parallel-across-the-method Runge-Kutta integrators with diagonal Butcher tables go back to the 1990s [14,15]. They were ultimately abandoned as the resulting methods lacked accuracy and stability. More successful and closely related to parallel SDC were iterated Runge-Kutta methods [13]. Parallel SDC as a method was first described by Speck in 2018 [28], relying on numerical optimization to find good parameters. Recently, an analytic approach yielded an improved method that could outperform both the previously published iterated RKM as well as parallel SDC with numerically optimized parameters [3]. However, in these demonstrations, parallel computational cost is only modeled and neither a parallel implementation is discussed nor are runtimes or speedup measured. The present paper fills this gap.

There are also a few papers that investigate the application of other variants of SDC to atmospheric modeling. The first is Jia et al. [16], showing that a serial SDC based on implicit Euler provides a high order integrator for a variety of meteorological test cases, one of them being the nonlinear evolution of a barotropic instability by Galewsky [8] we also use in this paper. Stability and accuracy of an implicit-explicit split SDC variant is studied for the linear Boussinesq equations by Speck and Ruprecht [26]. Hamon et al. [12] investigate performance of

a parallel-across-the-steps variant of SDC for the shallow water equation on a sphere.

A hybrid version between parallel-across-the-steps and parallel-across-the-method SDC are revisionist integral corrections or RIDC [22], which pipeline updates over a few steps. An attempt to speed up the operational ocean model FESOM2 using the parallel-across-the-steps integration method Parareal was very recently published [24,25] but, because of the complexities of building a coarse model, with only limited success. Overviews of parallel-in-time literature are given by Gander [9] and Ong and Schroder [23].

3 Models

We briefly sketch the two codes for which we benchmark parallel SDC with a focus on numerical time-stepping. The first model is the ocean part **ICON-0** of the operational earth system model **ICON**, the second is **SWEET**, a research code design for fast exploration of time stepping methods for geophysical fluid dynamics.

3.1 ICON-0

The Icosahedral Nonhydrostatic Weather and Climate Model (**ICON**) [30,32] is the earth system modeling framework of the Max Planck Institute for Meteorology (MPI-M), the German Weather Service (DWD), the German Climate Computing Center (DKRZ), and the Karlsruhe Institute of Technology (KIT). It is used both for research and operational weather forecasts. **ICON** supports different hybrid parallelization modes for scalability, including Message Passing Interface (MPI) for distributed memory computations, **OpenMP** for shared memory parallelism and **OpenACC** for GPUs. In this work, we will focus on pure, nested **OpenMP** parallelization on a single node.

ICON-0 is the ocean-sea ice component of **ICON**. It solves the hydrostatic Boussinesq equations of large-scale ocean dynamics with a free surface, also referred to as the primitive equations of large-scale ocean dynamics [17,19]. A special case of this complex dynamical system are the shallow water equations (SWE), which we will use as benchmark model. For the velocity \mathbf{v} , the fluid thickness η , the vertical component of the vorticity $\omega = \mathbf{k} \cdot \text{curl}(\mathbf{v}_1 \ \mathbf{v}_2 \ 0)^\top = \partial_x \mathbf{v}_2 - \partial_y \mathbf{v}_1$ and the bottom topography b , the SWE in inviscid, vector invariant form [20] read

$$\partial_t \mathbf{v} + g \nabla(\eta + b) = -(f + \omega) \mathbf{k} \times \mathbf{v} - \nabla |\mathbf{v}|^2 / 2, \quad (1a)$$

$$\partial_t \eta + \text{div}(\eta \mathbf{v}) = 0. \quad (1b)$$

Here g is the earth's gravity acceleration, f is the Coriolis parameter and \mathbf{k} the vector perpendicular to the earth's surface.

The discretization of (1) is described by Korn and Linadarkis [20, Section 3 and 4]. They develop a spatial discretization of the shallow water equations on possibly unstructured triangular Arakawa C-grids [1,2] that preserves the structure of the continuous equations, with particular emphasis on conservation properties. This is achieved by a combination of ideas from Finite Element and Finite Volume methods as well as mimetic discretization.

Since we focus on time integration and parallel performance, we will omit the details of the space discretization. The full space discrete model is also given by Korn and Linadarkis [20, equation (40)]. We consider the following space discrete counterpart of (1) where the differential operators mimic discrete counterparts of their continuous originals

$$\partial_t \mathbf{v} + \overbrace{g \nabla_h (\eta + b)}^{N(\eta)} = \overbrace{-\mathcal{M}^{-1} \widehat{\mathcal{P}}^\dagger (f + \omega) \widehat{\mathcal{P}} \mathbf{v} - \nabla_h |\mathcal{P} \mathbf{v}|^2 / 2}_{\mathcal{G}(\mathbf{v})}, \quad (2a)$$

$$\partial_t \eta + \underbrace{\operatorname{div}_h (\mathcal{P}^\top \eta \mathcal{P} \mathbf{v})}_{D(\eta, \mathbf{v})} = 0. \quad (2b)$$

The linear operators $(\mathcal{P}, \widehat{\mathcal{P}}, \widehat{\mathcal{P}}^\dagger)$, $\mathcal{M} = \mathcal{P}^\top \mathcal{P}$ build an *admissible reconstruction* [20, Definition 6]. This is necessary because different variables are located at different positions on the grid, i.e., edges or cells. We emphasize that the implementation uses a lumped mass matrix, i.e., approximates $\mathcal{M}^{-1} \approx \mathbf{I}$. It has been shown that this only has a negligible effect on C-grids [18].

The standard time integration scheme in ICON-0 is the semi-implicit Adams–Bashforth-2 scheme (AB), which is commonly used in ocean dynamics [4,5,20]. Again, the details of the implementation are found in the literature [20, Section 5.4.2]. AB first predicts a velocity to be used in the free surface equation that is solved using a conjugate gradient (CG) method. Eventually, the new velocity is calculated as a correction of the prediction using the gradient of the new fluid thickness. We use classical notation from time integration and divide the time interval $[0, T]$ in equidistant time slices $[t_n, t_{n+1}]$ of length $\Delta t = t_{n+1} - t_n$. The approximate solutions at time t_n are denoted as \mathbf{v}_n and η_n , respectively, and thus the AB scheme reads:

$$\begin{aligned} \bar{\mathbf{v}}_{n+1} &= \mathbf{v}_n - \Delta t \frac{2}{5} N(\eta_n) + \Delta t \left(\frac{3}{2} + 0.1 \right) \mathcal{G}(\mathbf{v}_n) - \Delta t \left(\frac{1}{2} + 0.1 \right) \mathcal{G}(\mathbf{v}_{n-1}), \\ \eta_{n+1} - \left(\Delta t \frac{3}{5} \right)^2 D(\eta_n, N(\eta_{n+1})) &= \eta_n - \Delta t D\left(\eta_n, \frac{3}{5} \bar{\mathbf{v}}_{n+1} + \frac{2}{5} \mathbf{v}_n\right), \\ \mathbf{v}_{n+1} &= \bar{\mathbf{v}}_{n+1} - \Delta t \frac{3}{5} N(\eta_{n+1}). \end{aligned}$$

To summarize, the expression $N(\eta)$ is integrated implicitly, whereas the non-linear part $\mathcal{G}(\mathbf{v})$ uses explicit integration. For the expression $D(\eta, \mathbf{v})$, we use a mixture, i.e., explicit in η and implicit in \mathbf{v} .

3.2 SWEET

The *Shallow Water Equation Environment for Tests, Awesome!* (SWEET) [27] is a research software meant for fast exploration of time integration methods for

PDEs using global spectral methods (Fourier transform and spherical harmonics). In particular, it can be used to solve the SWE on the rotating sphere:

$$\begin{bmatrix} \frac{\partial \Phi}{\partial t} \\ \frac{\partial \mathbf{V}}{\partial t} \end{bmatrix} = \underbrace{\begin{bmatrix} -\bar{\Phi} \nabla \cdot \mathbf{V} \\ -\nabla \Phi \end{bmatrix}}_{L_g(U)} + \underbrace{\begin{bmatrix} 0 \\ -f \mathbf{k} \times \mathbf{V} \end{bmatrix}}_{L_c(U)} + \underbrace{\begin{bmatrix} -\mathbf{V} \cdot \nabla \Phi' \\ -\mathbf{V} \cdot \nabla \mathbf{V} \end{bmatrix}}_{N_a(U)} + \underbrace{\begin{bmatrix} -\nabla \Phi' \cdot \mathbf{V} \\ 0 \end{bmatrix}}_{N_d(U)}, \quad (4)$$

with \mathbf{V} the velocity, Φ the geopotential, \mathbf{k} the vector perpendicular to the earth's surface and f related to the Coriolis effect. **SWEET** considers those equations in their vorticity-divergence formulation in Fourier space, which means that the solution vector is $\hat{U} := [\hat{\Phi}', \hat{\zeta}, \hat{\rho}]^\top$, with Φ' the perturbation on the geopotential, ζ the vorticity and ρ the divergence. We refer to [11] for further details.

The right-hand side of (4) is split into different terms or *tendencies*, that each are related to specific physical processes. $L_g(U)$ is the gravitational-related linear part, directly related to a 1D wave equation. It requires fully implicit time-integration to avoid very restrictive time-step conditions as it models the behavior of fast frequency modes in the solution (gravity waves). $L_c(U)$ is the Coriolis effect part and is integrated explicitly, separately from the gravity modes. This splitting, also used in the ECMWF model, allows to use an implicit pentadiagonal solver for $L_g(U)$ that is very efficient and easy to parallelize. The $N_a(U)$ and $N_d(U)$ are non-linear terms that are usually treated explicitly, which require to transform the solution variables from Fourier space, evaluate the tendencies in real space, and transform back to Fourier space again. The evaluation of those terms is usually the most expensive part in any spectral-discretization based solver. In **SWEET**, the parallel FFT are done using the `fftw3` library. Parallelization of most vector computations, FFTs and implicit linear solves is done with `OpenMP`.

Out of the many time-integration schemes already available in **SWEET**, we choose as reference method a semi-implicit time integration scheme of order 2. It uses a second order Strang splitting, integrates $L_g(U)$ with a Crank-Nicholson scheme and uses an explicit second order Runge-Kutta scheme (Heun's method) for $L_c(U) + N_a(U) + N_d(U)$. We call this time-scheme **IMEX-o2**. The motivation is to have a reference time-scheme similar to the semi-implicit AB scheme used in **ICON-0**.

4 Parallel SDC

Spectral Deferred Corrections with fast-wave slow-wave IMEX splitting [26] integrate an initial value problem of the form

$$u'(t) = f_I(u(t), t) + f_E(u(t), t), \quad u(0) = u_0 \quad (5)$$

where f_I are the fast, linear dynamics to be integrated implicitly and f_E the slow, non-linear dynamics treated explicitly. In essence, SDC is an iterative procedure to approximate the solution of a collocation method, which can be seen as a fully implicit Runge-Kutta method with a dense Butcher table [3].

To summarize the approach, we denote by $0 \leq \tau_1 < \dots < \tau_M \leq 1$ the quadrature nodes of the collocation method applied on the interval $[t_n, t_{n+1}]$, and define u_m^k an approximate solution of (5) at node $m \in \{1, \dots, M\}$. Then IMEX SDC iteration (or sweep) reads

$$\begin{aligned} u_m^{k+1} = u_n + \Delta t \sum_{j=1}^M q_{m,j} f(u_j^k) + \Delta t \sum_{j=1}^{m-1} \Delta\tau_{j+1} [f_E(\tau_j, u_j^{k+1}) - f_E(\tau_j, u_j^k)] \\ + \Delta t \sum_{j=1}^m \Delta\tau_j [f_I(\tau_j, u_j^{k+1}) - f_I(\tau_j, u_j^k)] \end{aligned}$$

where $\Delta t = t_{n+1} - t_n$ is the time step size, q_{m_j} are the entries of the Butcher table of the collocation method and $\Delta\tau_{j+1} = \tau_{j+1} - \tau_j$ the distance between the nodes ($\Delta\tau_1 = 0$).

Weiser [31] realized that it is possible to replace the $\Delta\tau_j$ with algebraic parameters $q_{m,j}^\Delta$ with $q_{m,j}^\Delta = 0$ if $j < m$ to speed up convergence without changing the sweep-structure of SDC. Speck [28] then observed that if the parameters are chosen such that $q_{m,j}^\Delta = 0$ if $m \neq j$, the computation of all u_m^{k+1} can be parallelized over M threads.

In this paper, we use MIN-SR-FLEX diagonal coefficients for the fast linear term (varying between sweeps) [3] and zero coefficients for the slow non-linear term. Furthermore, we use SDC with $M = 4$ Radau nodes such that $\tau_M = 1$ and always perform $M = K$ iterations, with the initial guess on each node u_m^0 being a copy of the solution u_n at the start of the current time step.

4.1 SDC in ICON-0

Because ICON-0 does not directly rely on the form (5) of the initial value problem, some modifications to SDC need to be made. Parallel SDC in ICON-0 mirrors the three-step approach of the already implemented semi-implicit AB scheme (3). An SDC sweep in ICON-0 reads

$$\begin{aligned} \bar{\mathbf{v}}_m^{k+1} &= \mathbf{v}_n + \frac{\tau_m \Delta t}{k} \mathbf{N}(\eta_m^k) + \Delta t \sum_{j=1}^M q_{m,j} (\mathcal{G}(\mathbf{v}_j^k) - \mathbf{N}(\eta_j^k)), \\ \eta_m^{k+1} - \left(\frac{\tau_m \Delta t}{k}\right)^2 \mathbf{D}(\eta_m, \mathbf{N}(\eta_m^{k+1})) &= \eta_m - \frac{\tau_m \Delta t}{k} (\mathbf{D}(\eta_m, \bar{\mathbf{v}}_m^{k+1}) - \mathbf{D}(\eta_m, \mathbf{v}_m^k)) \\ &\quad - \Delta t \sum_{j=1}^M q_{m,j} \mathbf{D}(\eta_j^k, \mathbf{v}_j^k), \\ \mathbf{v}_m^{k+1} &= \bar{\mathbf{v}}_m^{k+1} - \frac{\tau_m \Delta t}{k} \mathbf{N}(\eta_m^{k+1}), \end{aligned}$$

for $m = 1, \dots, M$ and $k = 0, \dots, K - 1$. Here, we used the notation introduced in (2).

Note that in the last sweep, we only compute the contribution of the last node, as all other values are not relevant. Eventually, the iterates of the next time step are given as the final sweep iterates, i.e., $\mathbf{v}_{n+1} = \mathbf{v}_M^K$ and $\eta_{n+1} = \mathbf{v}_M^K$.

We use inexact iterative solves in every step to further improve SDC efficiency [29]. The idea is that in early sweeps, implicit solves need not yet be very accurate because the SDC solution is not yet accurate. As SDC converges and accuracy improves, the previous iterates will provide increasingly accurate starting values for the iterative scheme. To solve the implicit part of the time-stepping, we use a CG scheme with a given tolerance of 10^{-7} and additionally restrict the number of CG iterations to a maximum of 4 to ensure load balance.

4.2 SDC in SWEET

Using the MIN-SR-FLEX preconditioning of [3] for the implicit tendency $L_g(u)$, and a Picard preconditioning ($\mathbf{Q}_\Delta = 0$) for the explicit tendencies $L_c(u) + N_a(u) + N_d(u) := T_E(u)$, the SDC iteration is then

$$u_m^{k+1} - \frac{\tau_m \Delta t}{k+1} L_g(u_m^{k+1}) = u_0 + \Delta t \sum_{i=1}^M q_{m,j} T_E(u_i^k), \quad k \in \{0, \dots, K-1\}.$$

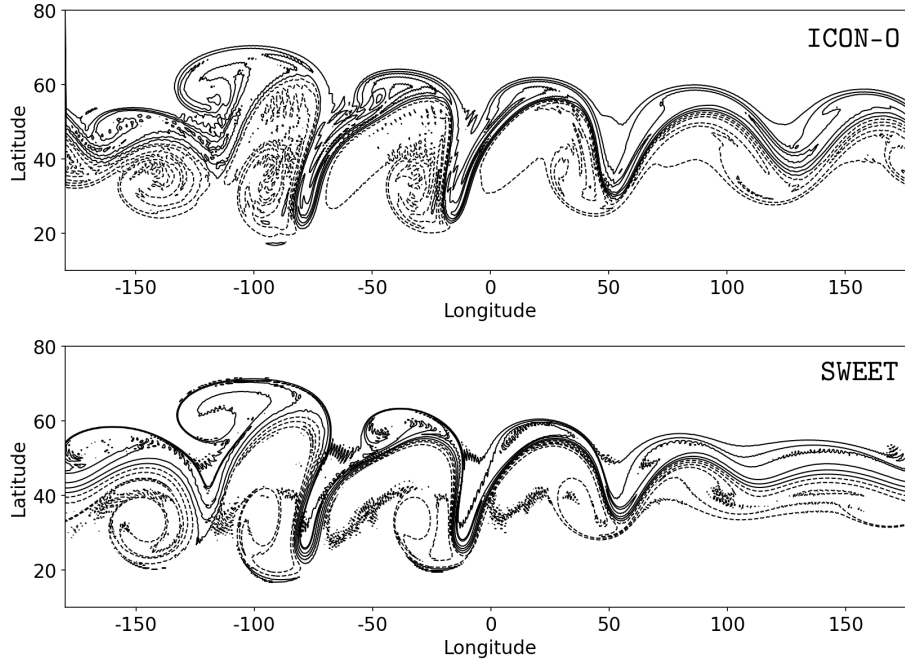
Note that since $\tau_M = 1$, we simply take u_M^K as final step solution, so one does not need to evaluate the tendencies for u_M^K .

5 Performance Model

We develop an elementary performance model to predict the speedup of pSDC, for both ICON-0 and SWEET. The computational costs are determined by two main operations: the explicit evaluation of the tendencies with cost c_E , and the implicit solve to compute the updated solution on one quadrature node with cost c_S . Both operations are present in ICON-0 and SWEET, and are performed during each sweeps. For the ICON-0 model, additional tendency evaluation of divergence terms are required due to the three-step approach, which generate an additional cost \tilde{c}_E during each sweep update.

Therefore, we develop our performance model as follows. To compute the SDC initial guess (using a copy of the initial time-step solution), only the tendencies evaluation with cost c_E is required. Then, within the sweeps, we need one explicit tendency evaluations c_E and one implicit solve c_S per nodes, which can be parallelized. For the ICON-0 model, due to the three-step approach, each node requires an additional evaluation of (explicit) divergences, and we note this supplementary cost \tilde{c}_E (while within SWEET, we have $\tilde{c}_E = 0$). Then for the last sweep, we only perform the implicit solve (cost c_S) for the last node without any tendency evaluation. Table 1 summarizes the costs for sequential and parallel implementation, hence the theoretical speed-up for parallel over serial SDC

sweep	sequential	parallel
$k = 0$	c_E	c_E
$k = 1, \dots, K - 1$	$M(c_E + c_S + \tilde{c}_E)$	$c_E + c_S + \tilde{c}_E$
$k = K$	c_S	c_S

Table 1. Computational costs for sequential and time-parallel pSDC.**Fig. 1.** Vorticity contours for the Galewsky test case at the end of day 6.

using $K = M$ sweeps is

$$S = \frac{C_{\text{seq}}}{C_{\text{par}}} = \frac{1 + M(M - 1)\left(1 + \frac{\tilde{c}_E}{c_E + c_S}\right)}{1 + (M - 1)\left(1 + \frac{\tilde{c}_E}{c_E + c_S}\right)}.$$

For ICON-0, measurements suggest a value $\frac{\tilde{c}_E}{c_E + c_S} \approx 0.13$, which yields $S \approx 3.3$ with $M = 4$. For SWEET, since $\tilde{c}_E = 0$, $S = 3.25$, which does not depend on c_E and c_S . Note that in general, since $\lim_{\tilde{c}_E \rightarrow \infty} S = M$, the maximum ideal speedup of pSDC with this configuration is M .

6 Results

For the numerical experiments and performance demonstration, we choose the well-established Galewsky test case. The test starts with an equilibrium with

an additional perturbation that eventually develops into turbulent flow. For the detailed formulation, including the analytical expression of the initial state, we refer to the original work by Galwesky [8]. Experiments are run until the end of day 6, after which the flow quickly becomes fully turbulent. A picture of the vorticity computed with ICON-0 and SWEET is shown in fig. 1. The fields generally look very similar but with some noticeable differences near the right boundary, due to the different discretizations used in ICON-0 and SWEET.

6.1 Strong scaling of parallel SDC

We first investigate strong scalability of pSDC by running simulations on one compute node of JUWELS for ICON-0 and JUSUF for SWEET, increasing the number of `OpenMP` threads used in space and time while keeping the problem size fixed.

In fig. 2, we show the runtime for pSDC scaled by the number of time steps times the number of degrees-of-freedom. Green squares are for SDC with space parallelization only whereas orange circles are pSDC parallelized in time using 4 `OpenMP` threads times an increasing number of threads to parallelize in space. The x -coordinate corresponds to the total number of threads used. For each model, we note that the time-parallel speedup of pSDC without space parallelization is close to values of $S = 3.3$ for ICON-0 and $S = 3.25$ for SWEET predicted by our performance model. For ICON-0 we achieve a speed-up of approximately 3.1, for SWEET a slightly smaller speed-up of 2.9.

Scaled runtime is observed for two spatial grid sizes, one with a reference resolution for the problem of interest (fig. 2 top), and one with a coarser resolution for comparison. For ICON-0, using time parallelization in pSDC allows for a greater reduction of wall-clock time compared to exclusive space parallelization in both cases. For SWEET, time parallelization has very little benefit over exclusive space parallelization. This is because of the high efficiency of parallelization of the spatial FFT used in SWEET's spectral discretization. However, for a smaller problem size (bottom), as space parallelization scales less efficiently, time parallelization does minimally reduce wall-clock time for pSDC.

We also compare with the scaled wall-clock time of the reference time integration schemes for each model, AB for ICON-0 and IMEX for SWEET. In both cases, the cost of a time-step is about a factor of ten smaller for the reference schemes than for pSDC. However, the better stability of SDC allows to take much larger and thus fewer time steps. To become competitive, SDC needs to be able to integrate with the same accuracy as AB/IMEX with a factor of ten fewer steps. The next section demonstrates that this can often be achieved for medium to high accuracies.

6.2 Work precision

Figure 3 shows work (measured in runtime) against precision (measured in the L^∞ - L^2 error of the vorticity) for 48 `OpenMP` threads for ICON-0 (left) and 64 `OpenMP` threads for SWEET (right). In ICON-0, for accuracies below 4 percent, we

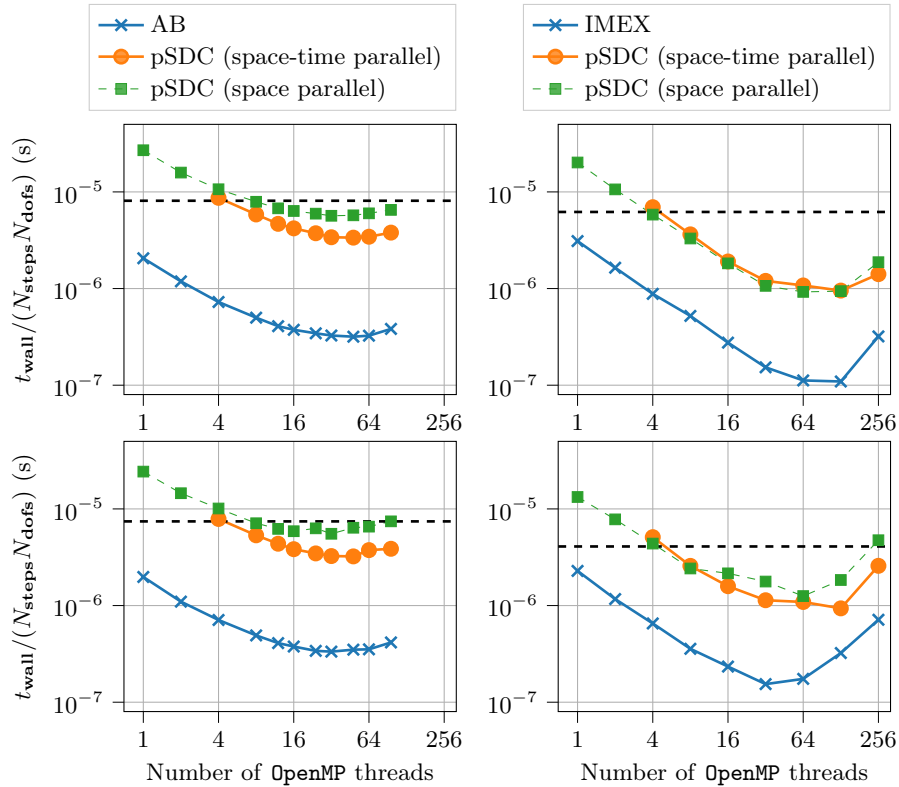


Fig. 2. Strong scaling tests for *ICON-0* (left) and *SWEET* (right). Top: using a problem size $N_{\text{dofs}} = 163842$ with *ICON-0* and $N_{\text{dofs}} = 512^2 = 262144$ with *SWEET*. Bottom: using a problem size $N_{\text{dofs}} = 40962$ with *ICON-0* and $N_{\text{dofs}} = 256^2 = 65536$ with *SWEET*. Ideal speedup of time-parallel pSDC determined using the performance model is drawn with the dashed black horizontal lines.

achieve faster time-to-solution with pSDC compared to AB. We emphasize that the maximal time-step for the respective methods are the coarsest possible ones, i.e., for larger time-steps the methods get unstable. As fig. 3 indicates, there is a small range of accuracies where the AB method performs best. Yet, we are confident that further optimization of the parallelization might push the pSDC line further to the left and lets us outperform AB for all regimes. We point out that with the pSDC we could even be faster than the coarsest possible AB scheme but only with a larger error. However, this might still be of interest, as meteorologists are usually interested in stability rather than accuracy. For *SWEET*, IMEX is more efficient for accuracies above 10^{-4} . Below that, first space parallel SDC and then space-time parallel SDC become the most efficient method. For both models, parallel SDC will provide shorter time-to-solution for medium to high accuracies.

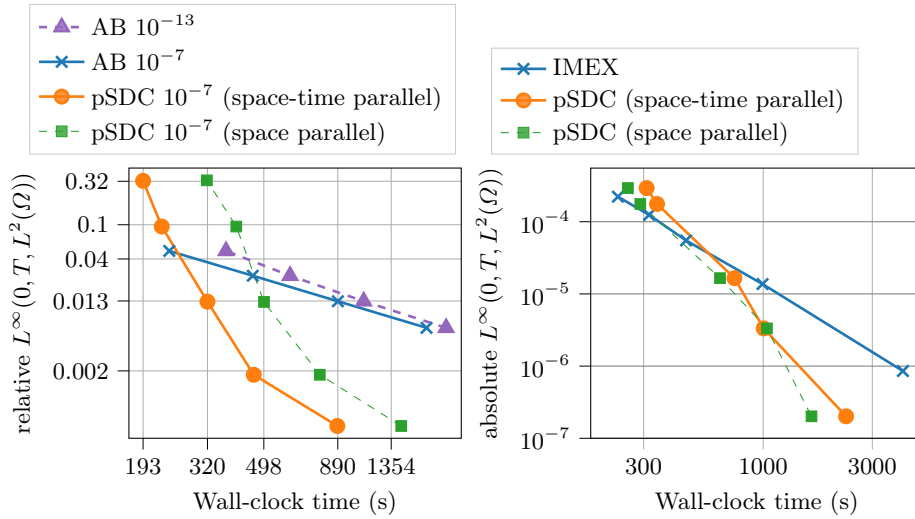


Fig. 3. Work-precision plot for ICON-0 (left) and SWEET (right). Left: using 48 threads, i.e., for AB and space only pSDC 48 in space and for space-time pSDC 4 in time and 12 in space. Various time-step sizes are used, for AB $\Delta t \in \{120, 60, 30, 15\}$ (s) and for pSDC $\Delta t \in \{1500, 1200, 960, 600, 300\}$ (s). AB is shown with CG tolerances of 10^{-13} and 10^{-7} , pSDC uses 10^{-7} . Right : using 64 threads for IMEX and pSDC (space), and nested parallelization with 32 threads in space and 4 threads in time for pSDC (space-time). Various time-step sizes are used, for IMEX $\Delta t \in \{60, \dots, 3.75\}$ (s) and for pSDC $\Delta t \in \{450, \dots, 60\}$ (s)

6.3 Speedup

Figure 4 (left) shows speedup for the different methods calibrated to provide an accuracy of around 0.013 in ICON-0. For the AB method, this means a time-step of 30 seconds while for pSDC we can use a time step size of 960 seconds. Since AB with two threads for loop parallelization is the default configuration in ICON-0, we use that as the reference to compute speedup. Replacing AB with space-parallel only SDC already provides a speedup of about two because the much larger time step that SDC can take more than compensates for the increased computing cost in each step. Adding more `OpenMP` threads to the loop parallelization provides additional speedup, up to around six for 32 threads. However, using nested `OpenMP` with the SDC parallelization as outer loop and ICON-0's existing loop parallelization as inner provides the best performance. Speedup for 32 `OpenMP` threads increase to more than 10.

For SWEET, speedups are shown in fig. 4 (right) for methods calibrated for an absolute accuracy of approximately $1.5 \cdot 10^{-5}$. Again, using SDC provides significant speedup over the IMEX base method. Here, however, there is little difference in performance between using space-only loop parallelization or a nested space-time approach. Both cases provide a maximum speedup of around

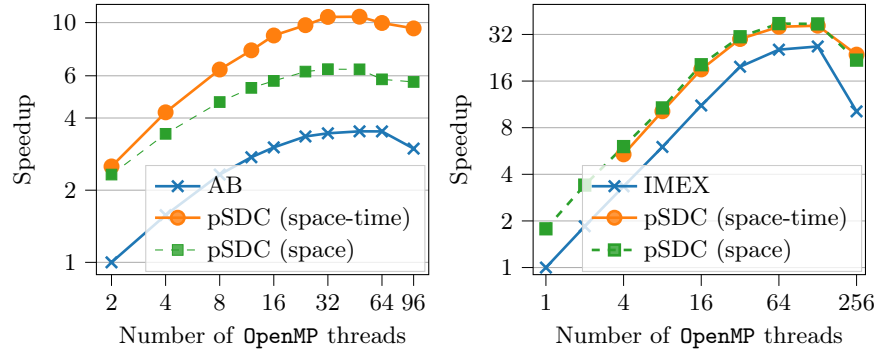


Fig. 4. Speedup of pSDC compared to reference time-integration schemes for a similar accuracy. Left: for *ICON-0*, comparing AB ($\Delta t = 30$ s) and pSDC ($\Delta t = 960$ s) at similar relative accuracy of ≈ 0.013 , using AB with 2 *OpenMP* threads (base configuration in *ICON-0*) as base method for speed-up. Right: for *SWEET*, comparing IMEX ($\Delta t = 15$ s) and pSDC ($\Delta t = 180$ s) at similar absolute accuracy of $\approx 1.5 \cdot 10^{-5}$.

256 for 64 threads with minimal difference in performance, which is due to the space parallelization in *SWEET* scaling better for this space grid size (cf. discussion in Section 6.1).

7 Discussion and outlook

This paper presents a shared memory parallel implementation of parallel-across-the-methods spectral deferred corrections. We demonstrate parallel speedup for two established simulation codes. In the operational ocean model *ICON-0*, a modified SDC implementation is used, adapted to the existing time-stepping infrastructure, whereas the standard formulation of SDC is implemented in the research code *SWEET*. For both implementations, theoretical considerations predict a speed-up of around 3.25 over serial SDC. In our implementations we reach speed-ups of 3.1 for *ICON-0* and 2.9 for *SWEET*. In both codes, SDC delivers shorter time-to-solution than the standard AB/IMEX methods for medium to high accuracies. Furthermore, we demonstrate that a nested *OpenMP* implementation in *ICON-0* with parallel SDC as outer and multi-threading of mesh operations as inner loop increases speedup significantly. By contrast, in *SWEET*, space-only and space-time parallelization perform almost identically. This illustrates that the benefits that can be gained from parallel SDC do heavily depend not only on implementation but also on the used spatial discretization. While parallel SDC might struggle to accelerate (pseudo)-spectral methods like the ones used in *SWEET*, it seems to be better suited to work in combination with mesh-based finite volume methods used in *ICON-0*.

The next step is to combine the proposed parallel-in-time scheme with the MPI parallelization. Only a hybrid parallelization approach will allow scalability to climatologically relevant scales. Moreover, the theoretical understanding

of pSDC may improve further since we mostly adopted parameters that were derived for purely implicit schemes. Further improvements to the optimized parameters may be possible for the IMEX-type approach used here.

Disclosure of Interests. The authors have no competing interests to declare that are relevant to the content of this article.

References

1. Arakawa, A., Hsu, Y.J.: Energy conserving and potential-*enstrophy* dissipating schemes for the shallow water equations. *Monthly Weather Review* **118**(10), 1960 – 1969 (1990)
2. Arakawa, A., Lamb, V.: A potential *enstrophy* and energy conserving scheme for the shallow water equations. *Monthly Weather Review* **109**(1), 18 – 36 (1981)
3. Čaklović, G., Lunet, T., Götschel, S., Ruprecht, D.: Improving parallelism across the method for spectral deferred correction (2024), in preparation
4. Campin, J.M., Adcroft, A., Hill, C., Marshall, J.: Conservation of properties in a free-surface model. *Ocean Modelling* **6**(3), 221–244 (2004)
5. Danilov, S., Sidorenko, D., Wang, Q., Jung, T.: The finite-volume sea ice–ocean model (FESOM2). *Geoscientific Model Development* **10**(2), 765–789 (2017)
6. Emmett, M., Minion, M.L.: Toward an Efficient Parallel in Time Method for Partial Differential Equations. *Communications in Applied Mathematics and Computational Science* **7**, 105–132 (2012)
7. Falgout, R.D., Friedhoff, S., Kolev, T.V., MacLachlan, S.P., Schroder, J.B.: Parallel time integration with multigrid. *SIAM Journal on Scientific Computing* **36**, C635–C661 (2014)
8. Galewsky, J., Scott, R.K., Polvani, L.M.: An initial-value problem for testing numerical models of the global shallow-water equations. *Tellus A: Dynamic Meteorology and Oceanography* **56**(5), 429–440 (2004)
9. Gander, M.J.: 50 years of Time Parallel Time Integration. In: *Multiple Shooting and Time Domain Decomposition*. Springer (2015)
10. Gear, C.W.: Parallel methods for ordinary differential equations. *CALCOLO* **25**(1–2), 1–20 (1988)
11. Hack, J.J., Jakob, R.: Description of a global shallow water model based on the spectral transform method (1992)
12. Hamon, F.P., Schreiber, M., Minion, M.L.: Parallel-in-time multi-level integration of the shallow-water equations on the rotating sphere. *Journal of Computational Physics* **407**, 109210 (apr 2020)
13. van der Houwen, P.J., Sommeijer, B.P.: Iterated Runge–Kutta methods on parallel computers. *SIAM Journal on Scientific and Statistical Computing* **12**(5), 1000–1028 (1991)
14. Iserles, A., Nørsett, S.P.: On the theory of parallel Runge–Kutta methods. *IMA Journal of Numerical Analysis* **10**(4), 463–488 (1990)
15. Jackson, K.R.: A survey of parallel numerical methods for initial value problems for ordinary differential equations. *IEEE Transactions on Magnetics* **27**, 3792–3797 (1991)
16. Jia, J., Hill, J.C., Evans, K.J., Fann, G.I., Taylor, M.A.: A spectral deferred correction method applied to the shallow water equations on a sphere. *Monthly Weather Review* **141**, 3435–3449 (2014)

17. Korn, P., Brüggemann, N., Jungclaus, J.H., Lorenz, S.J., Gutjahr, O., Haak, H., Linardakis, L., Mehlmann, C., Mikolajewicz, U., Notz, D., Putrasahan, D.A., Singh, V., von Storch, J.S., Zhu, X., Marotzke, J.: ICON-O: The ocean component of the ICON earth system model—global simulation characteristics and local telescoping capability. *Journal of Advances in Modeling Earth Systems* **14**(10), e2021MS002952 (2022)
18. Korn, P., Danilov, S.: Elementary dispersion analysis of some mimetic discretizations on triangular C-grids. *Journal of Computational Physics* **330**, 156–172 (2017)
19. Korn, P.: Formulation of an unstructured grid model for global ocean dynamics. *J. Comput. Phys.* **339**, 525–552 (2017)
20. Korn, P., Linardakis, L.: A conservative discretization of the shallow-water equations on triangular grids. *J. Comput. Phys.* **375**, 871–900 (2018)
21. Lions, J.L., Maday, Y., Turinici, G.: A "parareal" in time discretization of PDE's. *Comptes Rendus de l'Académie des Sciences - Series I - Mathematics* **332**, 661–668 (2001)
22. Ong, B.W., Haynes, R.D., Ladd, K.: Algorithm 965: RIDC methods: A family of parallel time integrators. *ACM Trans. Math. Softw.* **43**(1), 8:1–8:13 (2016)
23. Ong, B.W., Schroder, J.B.: Applications of time parallelization. *Computing and Visualization in Science* **23**(1-4) (sep 2020)
24. Philippi, B., Slawig, T.: A micro-macro parareal implementation for the ocean-circulation model FESOM2. *arXiv:2306.17269v1 [math.NA]* (2023)
25. Philippi, B., Slawig, T.: The parareal algorithm applied to the FESOM 2 ocean circulation model. *arXiv:2208.07598v1 [math.NA]* (2022)
26. Ruprecht, D., Speck, R.: Spectral deferred corrections with fast-wave slow-wave splitting. *SIAM J. Sci. Comput.* **38**(4), A2535–A2557 (2016)
27. Schreiber, M., Peixoto, P.S., Haut, T., Wingate, B.: Beyond spatial scalability limitations with a massively parallel method for linear oscillatory problems. *The International Journal of High Performance Computing Applications* **32**(6), 913–933 (2018)
28. Speck, R.: Parallelizing spectral deferred corrections across the method. *Computing and Visualization in Science* (2018)
29. Speck, R., Ruprecht, D., Minion, M., Emmett, M., Krause, R.: Inexact spectral deferred corrections. In: Dickopf, T., Gander, J.M., Halpern, L., Krause, R., Pavarino, F.L. (eds.) *Domain Decomposition Methods in Science and Engineering XXII*. pp. 389–396. Springer International Publishing (2016)
30. Wan, H., Giorgetta, M.A., Zängl, G., Restelli, M., Majewski, D., Bonaventura, L., Fröhlich, K., Reinert, D., Rípodas, P., Kornbluh, L., Förstner, J.: The ICON-1.2 hydrostatic atmospheric dynamical core on triangular grids – part 1: Formulation and performance of the baseline version. *Geoscientific Model Development* **6**(3), 735–763 (2013)
31. Weiser, M.: Faster SDC convergence on non-equidistant grids by DIRK sweeps. *BIT Numerical Mathematics* **55**(4), 1219–1241 (2014)
32. Zängl, G., Reinert, D., Rípodas, P., Baldauf, M.: The ICON (icosahedral non-hydrostatic) modelling framework of DWD and MPI-M: Description of the non-hydrostatic dynamical core. *Quarterly Journal of the Royal Meteorological Society* **141**(687), 563–579 (2015)